A plasmaspheric mass density model and constraints on its heavy ion concentration

D. Berube and M. B. Moldwin[1]
Department of Earth and Space Sciences, University of California, Los Angeles, California, USA

S. F. Fung and J. L. Green
NASA Goddard Space Flight Center, Greenbelt, Maryland, USA

Received 14 July 2004; revised 14 January 2005; accepted 28 January 2005; published 22 April 2005.

[1] The first empirical model of the equatorial mass density of the plasmasphere is constructed using ground-based ULF wave diagnostics. Plasmaspheric mass density between $L = 1.7$ and $L = 3.2$ has been determined using over 5200 hours of data from pairs of stations in the MEASURE array of ground magnetometers. The least squares fit to the data as a function of L shows that mass density falls logarithmically with L. Average ion mass as a function of L is also estimated by combining the mass density model with plasmaspheric electron density profiles determined from the IMAGE Radio Plasma Imager (RPI). Additionally, we use the RPI electron density database to examine how the average ion mass changes under different levels of geomagnetic activity. We find that average ion mass is greatest under the most disturbed conditions. This result indicates that heavy ion concentrations (percent by number) are enhanced during large geomagnetic disturbances. We also find that the average ion mass increases with increasing L (below $L = 3.2$), indicating the presence of a heavy ion torus during disturbed times. Heavy ions must play an important role in storm-time plasmaspheric dynamics. The average ion mass is also used to constrain the concentrations of He^+ and O^+. Estimates of the He^+ concentration determined this way may be useful for interpreting IMAGE Extreme Ultraviolet Imager (EUV) images.

Citation: Berube, D., M. B. Moldwin, S. F. Fung, and J. L. Green (2005), A plasmaspheric mass density model and constraints on its heavy ion concentration, *J. Geophys. Res.*, *110*, A04212, doi:10.1029/2004JA010684.

1. Introduction

[2] Many studies have been performed using spacecraft data and VLF whistlers to determine the equatorial electron density profile of the inner magnetosphere [e.g, *Chappell*, 1972; *Farrugia et al.*, 1989; *Carpenter and Anderson*, 1992; *Fung et al.*, 2001; *Sheeley et al.*, 2001]. The usual result is that plasmaspheric equatorial electron density $(n_e)_{eq}$ ranges from hundreds to many thousands per cubic centimeter and decreases with radial distance from the Earth. *Carpenter and Anderson* [1992] use a linear fit to the log electron density. Diurnal [e.g., *Park et al.*, 1978], annual [e.g., *Clilverd et al.*, 1991], and storm-related [e.g., *Park*, 1973; *Park*, 1974] variations of the total electron plasma density have all been observed.

[3] The mass density and composition of the plasmasphere are not as well known, particularly the inner plasmasphere ($L < 3$). This is because satellites pass through this region quickly and spacecraft charging effects make direct measurements of the dense, low-energy plasma difficult [*Moldwin*, 1997]. Many mass density and composition observations of the plasmasphere have come from the DE-1, GEOS-1, ISEE-1, and OGO-5 spacecraft [e.g., *Horwitz et al.*, 1984; *Farrugia et al.*, 1989; *Baugher et al.*, 1980; *Chappell et al.*, 1970; *Chappell*, 1972]. Several studies have found that the relative abundances of heavy ions in the plasmasphere vary greatly. *Craven et al.* [1997] reported typical He^+ to H^+ ratios in the plasmasphere of $\sim$0.03–0.3, implying He^+ abundances of $\sim$3–23 percent by number, assuming no other heavy ions are present. *Horwitz et al.* [1984] found that in the aftermath of a storm, O^+ density could become comparable to H^+ density in the plasmasphere.

[4] Techniques exist for remotely sensing the mass density along closed magnetic field lines which involve using pairs of ground-based magnetometers to measure field line resonance frequencies (also referred to as eigenfrequencies). These frequencies can then be used to infer the mass density along the magnetic field, much like the mass density along a string fixed at both ends can be determined from its harmonic frequencies [*Schultz*, 1996; *Denton and Gallagher*, 2000]. Two of these techniques are the power ratio technique [*Baransky et al.*, 1985, 1989] and the cross-phase technique [*Waters et al.*, 1991, 1994]. An automated method for

[1]Also at Institute of Geophysics and Planetary Physics, University of California, Los Angeles, California, USA.

0148-0227/05/2004JA010684$09.00

Table 1. MEASURE Stations Used in This Study

Station Name	Abbr.	Geographic Lat., deg	Geographic Lon., deg
Ottawa, Canada	OTT	45.40 N	75.50 W
Clarkson University, Potsdam, NY	CLK	44.70 N	75.00 W
Boston University, Millstone Hill, MA	MSH	42.60 N	71.48 W
Applied Physics Lab, Laurel, MD	APL	39.17 N	76.88 W
Dark Sky Observatory, Boone, NC	DSO	36.25 N	81.40 W
Jacksonville University, Jacksonville, FL	JAX	30.35 N	81.60 W
Bullcreek Observatory, Melbourne, FL	FIT	28.07 N	80.95 W

determining field line eigenfrequencies which uses both techniques has been developed by *Berube et al.* [2003]. This new routine allows the analysis of large amounts of data and hence the development of a mass density database for the plasmasphere.

[5] In this study a model of the equatorial mass density of the plasmasphere using ULF (Ultra Low Frequency) field line resonances is constructed using data from pairs of ground-based magnetometers. The mass density model is then combined with IMAGE Radio Plasma Imager (RPI) electron density measurements [*Fung et al.*, 2001] to determine the average ion mass and estimate the maximum concentration of heavy ions in the plasmasphere.

2. Equatorial Mass Density Model

[6] The MEASURE array of ground magnetometers (http://measure.igpp.ucla.edu) is located along the east coast of the United States and consists of ten stations covering L = 1.68 to L = 3.18. Data from seven of the stations (six pairs) were used in this study. The stations are listed in Table 1. Field line eigenfrequencies have been determined using the method of *Berube et al.* [2003] for approximately 5200 hours of data from six pairs of stations in the array from the years 1999–2001 (the station pairs have midpoints at L = 1.74, 1.99, 2.30, 2.57, 2.89, and 3.12). The uncertainty associated with the selected frequencies is typically 1–2 mHz and is discussed in detail by *Berube et al.* [2003]. Hourly averaged mass density is computed from field line eigenfrequencies. We assume a dipole geomagnetic field and a r^{-3} dependence of density along the field line, where r is radial distance from the Earth. Mass density is computed using the results of *Schulz* [1996], who provides a relationship between field line resonant frequencies and mass density. Field line resonances are primarily present only during the daytime due to the reduced conductivity of the nightside ionosphere. Ninety-five percent of the field line resonance data used in this study is in the range 0600–1800 MLT. Therefore this model is only valid for the dayside sector.

[7] Figure 1 shows the hourly mass density estimates obtained for each of the six pairs of magnetometers plotted as a function of L. The line is the least squares linear fit to the log average density at each L sampled ($1.7 < L < 3.1$). It is given by the expression

$$\rho_{eq}(L) = 10^{-0.67L+5.1}. \quad (1)$$

The equation represents the average mass density of the dayside plasmasphere, since it includes all levels of activity. For quiet times ($-9 < Dst < -3$ nT), 1098 hours of data were available. The density is given by the following equation:

$$\rho_{eq}(L) = 10^{-0.65L+5.1}. \quad (2)$$

For the most disturbed times ($Dst < -100$ nT), 260 hours of data were available,

$$\rho_{eq}(L) = 10^{-0.74L+5.5}. \quad (3)$$

The ranges of *Dst* were chosen to be consistent with the ranges used in the *Fung et al.* [2001] model. Roughly three quarters of the data fall into the "moderately disturbed" category. Therefore the fit to the moderately disturbed data is nearly the same as the fit to all the data and has not been included here. It should be noted that both models use the current *Dst* index rather than some time-delayed value. The uncertainties in the parameters of each fit were determined using standard error propagation techniques [*Bevington and Robinson*, 1992] and are listed in Table 2.

3. Radio Plasma Imager Electron Density

[8] Here we review the methodology and relevant results of the *Fung et al.* [2001] statistical study of plasmaspheric electron density. The Radio Plasma Imager (RPI) on board the IMAGE satellite makes in situ measurements of

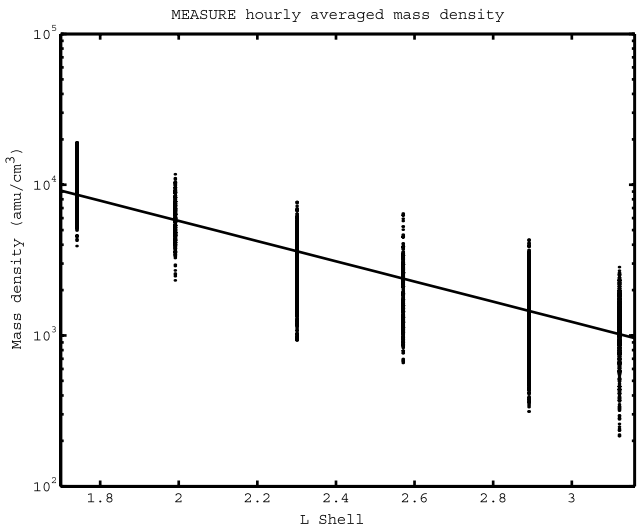

Figure 1. Average plasmaspheric mass density from six pairs of stations in the MEASURE array. The line represents the least squares linear fit to the mean density at each L and is described by equation (1) in the text.

Table 2. Parameters of the Least Squares Fit to Observed Hourly Averaged Mass Density Data[a]

Data	Hours Avail.	c1	σc1	c2	σc2
All times	5247	−0.67	+0.03 −0.08	5.1	+0.1 −0.1
Quiet (−9 < *Dst* < −3)	1098	−0.65	+0.10 −0.05	5.1	+0.1 −0.1
Disturbed (*Dst* < −100)	260	−0.74	+0.05 −0.08	5.5	+0.1 −0.1

[a]The model values are linear fits to the log average hourly density at each L. Here $\rho(L) = 10^{(c1+\sigma c1)L + (c2+\sigma c2)}$. The density data are from six pairs of stations in the MEASURE array in the range $1.7 < L < 3.1$.

magnetospheric electron density by detecting plasma resonances at the local upper hybrid frequency $f_{uh}^2 = f_p^2 + f_{ce}^2$, where f_p and f_{ce} are the local plasma and gyrofrequencies, respectively [*Reinisch et al.*, 2001]. The electron gyrofrequency is estimated using the T96 magnetic field model [*Tsyganenko*, 1995], and the electron density is computed from the resulting plasma frequency. Using all RPI electron density measurements between May 2000 and May 2001 taken when IMAGE was less than 20 degrees in latitude from the geomagnetic equator, *Fung et al.* [2001] assembled a database of electron density binned by spacecraft location in local time and L and geomagnetic indices such as *Dst*. The expressions for electron density presented here are determined by performing a least squares fit to the binned data between $2 < L < 5$. Figure 2 shows all the data plotted versus L shell. The line is the least squares linear fit to the log electron density. For all of the data,

$$n_{eq}(L) = 10^{-0.66L+4.89}. \quad (4)$$

For quiet times ($-9 < Dst < -3$ nT),

$$n_{eq}(L) = 10^{-0.51L+4.56} \quad (5)$$

and for disturbed times ($Dst < -100$ nT),

$$n_{eq}(L) = 10^{-1.04L+5.41}. \quad (6)$$

In comparison with (4), *Carpenter and Anderson* [1992] find $n_{eq}(L) = 10^{(-0.315L+3.9)}$, a dependence less steep than (4), though the value of n_{eq} at $L = 3$ (near the outer limit of our mass density data) is almost the same. *Sheeley et al.* [2001] use a power law dependence, $n_{eq} = 1390(3/L)^{4.83}$, but if we equate $n_{eq}(L)$ and its derivative at $L = 3$ to the form 10^{c1L+c2} and its derivative at $L = 3$, respectively, we find that the Sheeley result can be written as $n_{eq}(L) = 10^{(-0.7L+5.2)}$, which is quite similar to the dependence in (4) or (1).

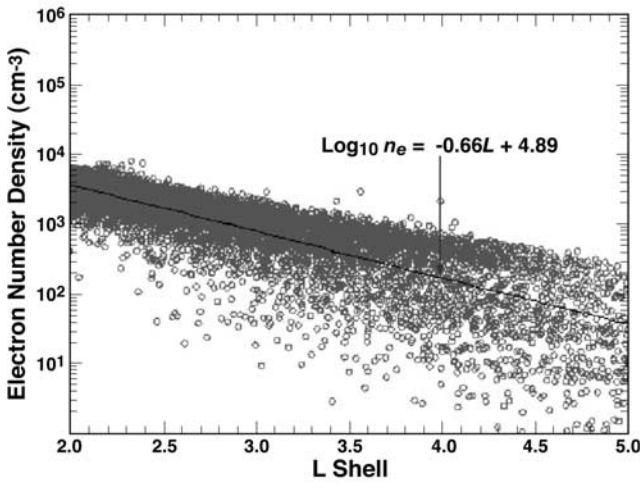

Figure 2. Electron number density measured by IMAGE RPI within 20 degrees latitude of the geomagnetic equator for $2 < L < 5$. The line represents the least squares fit to the log density (equation (4) in the text).

4. Average Ion Mass and Composition of the Plasmasphere

[9] The average ion mass (assumed to be singly charged) can be determined from the mass and electron density profiles since $M_{avg} = \rho_{eq}/n_{eq}$. Figure 3 is a plot of the average ion mass determined from the mass density and electron density models described above. The bottom solid line (x markers) represents the average ion mass for quiet geomagnetic conditions. The top solid line (asterisk markers) represents the disturbed-time profile. The dashed lines represent the uncertainty associated with each quantity and are based on the uncertainties in the parameters of the least squares fit to the data (see Table 2). The overall profile of average ion mass is not plotted in Figure 3, since it is nearly identical to the quiet-time profile. The overall

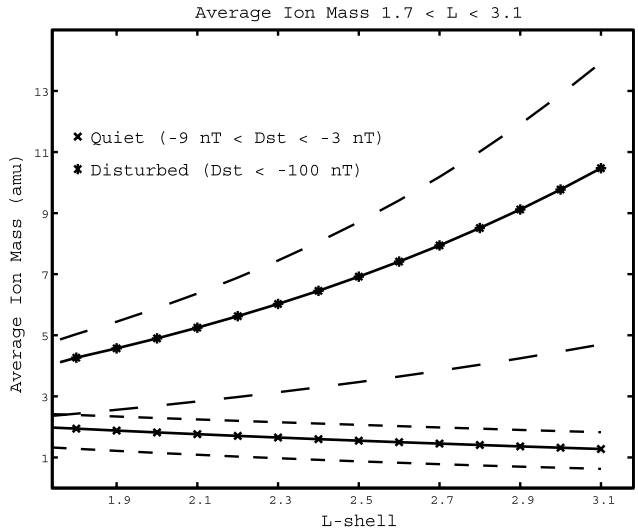

Figure 3. Average ion mass derived from equatorial mass and electron density models. The solid lines represent the ion mass for low levels of geomagnetic activity (X) and highly disturbed levels (*). The dashed lines represent the uncertainty in each quantity, based on the uncertainties in the parameters of the least squares fit to the data. The average ion mass for all levels of activity is not plotted here because the curve lies nearly on top of the quiet-time curve.

Table 3. Maximum Heavy Ion Concentrations Determined From Ground-Data-Derived Mass Density Model and RPI in Situ Electron Density Profiles, Using Equation (7) From the Text and Assuming Only One Heavy Ion Species is Present for Each Case[a]

	He^+		O^+	
	$L = 2$	$L = 3$	$L = 2$	$L = 3$
All data	40%	45%	8.0%	8.9%
Quiet times	43%	29%	8.6%	5.7%
Disturbed times	>100%	>100%	25%	62%

[a]Values >100% for He^+ during disturbed times indicate that He^+ alone cannot account for the mass density. There must be an additional heavy ion, probably O^+.

and quiet-time profiles are close to unity for $2 < L < 3$ suggesting that on average, the plasmasphere is made up of mostly H^+. For the most disturbed times ($Dst < -100$ nT) the average ion mass is significantly larger and increasing with increasing L. This suggests that during storms, a considerable number of heavy ions are present in the plasmasphere, with more heavy ions at larger L, indicating the presence of a heavy ion torus in the plasmasphere. Since the major constituents of the plasmasphere are H^+, He^+, and O^+, their concentrations can be estimated with the following relationship:

$$M_{avg} \cong m_{H^+}[\%H^+] + m_{He^+}[\%He^+] + m_{O^+}[\%O^+]. \quad (7)$$

If only one heavy ion species is assumed to be present, the maximum concentration of that species can be determined. For example, the upper limit on the average ion mass at $L = 2$ overall is approximately 2.2 a.m.u., implying a maximum He^+ concentration of 40% by number and a maximum of 8% for O^+. Table 3 shows maximum heavy ion concentrations determined this way for the entire data set, quiet times, and disturbed times. The maximum concentration is determined from the upper limit on average ion mass in each case. It should be stressed that this maximum determined this way only assumes one heavy ion species. Values of M_{avg} greater than 4 infer that there must be heavier ion species than He^+ present in order to explain the observed average ion mass.

5. Discussion

[10] The He^+ and O^+ concentrations in Table 3 are estimates based on the average mass and electron densities of the plasmasphere. The findings presented here agree well with the results of previous studies. For example, *Craven et al.* [1997], using DE-1 RIMS (Retarding Ion Mass Spectrometer) data, found He^+/H^+ ratios of $\sim 0.03-0.3$ (roughly 3–25 percent by number if we assume no other heavy ions are present). They also found that in general, the relative abundance of He^+/H^+ decreases with distance from the Earth, by an order of magnitude through the plasmasphere. Our findings are consistent with both these results for the quiet-time and overall plasmasphere. We find much higher heavy ion concentrations during disturbed times. Recently, *Dent et al.* [2003], using the same ground techniques as this study combined with simultaneous electron density measurements from IMAGE RPI and VLF whistler techniques, for a single case study, found quiet-time He^+ concentrations of 35–64 percent or O^+ concentrations of 7–13 percent for $L < 3.45$ and almost no heavy ions for $L > 3.45$. Our average results are slightly lower than their single event estimates, but the trend of smaller concentrations of heavy ions at higher L for quiet times is the same.

[11] As noted earlier, our observations indicate an increase in heavy ion concentration at midlatitudes during the main phase of a storm. The source of these ions is the ionosphere. During storms, particle precipitation intensifies and expands toward lower latitudes, heating the atmosphere and producing a large backsplash of energetic neutral oxygen, increasing heavy ion outflows [*Torr et al.*, 1974]. The increased heating of the atmosphere can also lead to the development of upward diffusion of heavy ions in the collisional F region of the ionosphere [*Yeh and Foster*, 1990]. Such outflows have been observed at $L \sim 2.5$ [see *Yeh and Foster*, 1990, and references therein]. These enhanced O^+ fluxes should be observed in the plasmasphere and ring current populations. Indeed, greatly increased concentrations of O^+ have been observed in the ring current [*Hamilton et al.*, 1988], and the results presented here are consistent with increased O^+ concentration in the plasmasphere.

[12] Independent estimates of He^+ in the magnetosphere are a necessary aid to the inversion of IMAGE Extreme Ultraviolet (EUV) images. Plasma mass density models such as the one presented here can be used to estimate the He^+ along the instrument's line of sight. However, in order to make such an estimate, one must assume (or somehow measure) relative heavy ion abundances. In a recent study, *Clilverd et al.* [2003] found for two events that changes in He^+ column abundance appear to correlate with changes in He^+ determined from ground-based ULF and VLF observations. As mentioned, matching of actual He^+ densities will require either assumed or measured O^+ relative abundance. Future studies will need to combine ground-based ULF wave estimations of mass density with in situ and VLF-derived electron densities and IMAGE EUV He^+ observations to create a clearer picture of the plasmasphere's composition.

[13] The model presented here is a first step toward a much more detailed empirical plasmaspheric mass density model. Each year, more ground magnetometer data become available, and longitudinal arrays of ground stations suited for measuring field line resonances are increasingly common. Future studies will incorporate data from multiple arrays spanning a wider range in latitude and longitude. This will allow local time variations in plasma mass density to be investigated. We will also be able to generate plasma mass density "maps" of the inner magnetosphere that can be used as input into ring current and magnetosphere/ionosphere coupling models.

[14] **Acknowledgments.** The MEASURE array is supported by NSF grant ATM-01-9223 and data are available at http://measure.igpp.ucla.edu. David Berube is supported by NASA Graduate Student Research Fellowship NASA NGT5-117.

[15] Arthur Richmond thanks Zoe Dent and Richard Denton for their assistance in evaluating this paper.

References

Baransky, L. N., J. E. Borovkov, M. B. Gokhberg, S. M. Krylov, and V. A. Troitskaya (1985), High resolution method of direct measurement of the magnetic field lines' eigenfrequencies, *Planet. Space Sci.*, *33*(12), 1369.

Baransky, L. N., S. P. Belokris, Y. E. Borovkov, M. B. Gokhberg, N. Federov, and C. A. Green (1989), Restoration of the meridional structure of geomagnetic pulsation fields from gradient measurements, *Planet. Space Sci.*, *37*(7), 859.

Baugher, C. R., C. R. Chappell, J. L. Horwitz, E. G. Shelley, and D. T. Young (1980), Initial thermal plasma observations from ISEE 1, *Geophys. Res. Lett.*, *7*, 657.

Berube, D., M. B. Moldwin, and J. M. Weygand (2003), An automated method for the detection of field line resonance frequencies using ground magnetometer techniques, *J. Geophys. Res.*, *108*(A9), 1348, doi:10.1029/2002JA009737.

Bevington, P. R., and D. K. Robinson (1992), Least-squares fit to a straight line, in *Data Reduction and Error Analysis for the Physical Sciences*, 2nd ed., pp. 96–114, chap. 6, McGraw-Hill, Boston.

Carpenter, D. L., and R. R. Anderson (1992), An ISEE/whistler model of equatorial electron density in the magnetosphere, *J. Geophys. Res.*, *97*(A2), 1097.

Chappell, C. R. (1972), Recent satellite measurements of the morphology and dynamics of the plasmasphere, *Rev. Geophys.*, *10*(4), 951.

Chappell, C. R., K. K. Harris, and G. Sharp (1970), A study on the influence of magnetic activity on the location of the plasmapause as measured by OGO 5, *J. Geophys. Res.*, *75*, 50.

Clilverd, M. A., A. J. Smith, and N. R. Thomson (1991), The annual variation in quiet time plasmaspheric electron density, determined from whistler mode group delays, *Planet. Space Sci.*, *39*(7), 1059.

Clilverd, M. A., et al. (2003), In situ and ground-based intercalibration measurements of plasma density at $L = 2.5$, *J. Geophys. Res.*, *108*(A10), 1365, doi:10.1029/2003JA009866.

Craven, P. D., D. L. Gallagher, and R. H. Comfort (1997), Relative concentration of He+ in the inner magnetosphere as observed by the DE1 retarding ion mass spectrometer, *J. Geophys Res.*, *102*(A2), 2279.

Dent, Z. C., I. R. Mann, F. W. Menk, J. Goldstein, C. R. Wilford, M. A. Clilverd, and L. G. Ozeke (2003), A coordinated ground-based and IMAGE satellite study of quiet-time plasmasphere density profiles, *Geophys. Res. Lett.*, *30*(12), 1600, doi:10.1029/2003GL016946.

Denton, R. E., and D. L. Gallagher (2000), Determining the mass density along magnetic field lines from toroidal eigenfrequencies, *J. Geophys. Res.*, *105*(A12), 27,717.

Farrugia, C. J., D. T. Young, J. Geiss, and H. Balsiger (1989), The composition, temperature, and density structure of cold ions in the quiet terrestrial plasmasphere: GEOS 1 results, *J. Geophys Res.*, *94*(A9), 11,865.

Fung, S. F., L. N. Garcia, J. L. Green, D. L. Gallagher, D. L. Carpenter, B. W. Reinisch, I. A. Galkin, G. Khmyrov, and B. R. Sandel (2001), Plasmaspheric electron density distributions sampled by radio plasma imager on the IMAGE satellite, *Eos Trans. AGU*, *82*(47), Fall Meet. Suppl., Abstract SM11A-0771.

Hamilton, D. C., G. Gloekler, F. M. Ipavich, B. Wilken, and W. Stuedmann (1988), Ring current development during the great geomagnetic storm of February, 1986, *J. Geophys. Res.*, *93*(A12), 14,343.

Horwitz, J. L., R. H. Comfort, and C. R. Chappell (1984), Thermal ion composition measurements of the formation of the new outer plasmasphere and double plasmapause during storm recovery phase, *Geophys. Res. Lett.*, *11*(8), 701.

Moldwin, M. B. (1997), Outer plasmaspheric properties: What we know from satellite data, *Space Sci. Rev.*, *80*, 181.

Park, C. G. (1973), Whistler observations of the depletion of the plasmasphere during a geomagnetic substorm, *J. Geophys. Res.*, *78*(4), 672.

Park, C. G. (1974), Some features of plasma distribution in the plasmasphere deduced from Antarctic whistlers, *J. Geophys. Res.*, *79*(1), 169.

Park, C. G., D. L. Carpenter, and D. B. Wiggin (1978), Electron density in the plasmasphere: Whistler data on solar cycle, annual, and diurnal variations, *J. Geophys. Res.*, *83*(A7), 3137.

Reinisch, B. W., et al. (2001), First results from the Radio Plasma Imager on IMAGE, *Geophys. Res. Lett.*, *28*(6), 1167.

Schulz, M. (1996), Eigenfrequencies of geomagnetic field lines and implications for plasma-density modeling, *J. Geophys. Res.*, *101*(A8), 17,385.

Sheeley, B. W., M. B. Moldwin, and H. K. Rassoul (2001), An empirical plasmasphere and trough density model: CRRES observations, *J. Geophys Res.*, *106*(A11), 25,631.

Torr, M. R., J. C. G. Walker, and D. G. Torr (1974), Escape of fast oxygen from the atmosphere during geomagnetic storms, *J. Geophys. Res.*, *79*, 5267.

Tsyganenko, N. A. (1995), Modeling the Earth's magnetospheric magnetic field confined within a realistic magnetopause, *J. Geophys. Res.*, *100*(A4), 5599.

Waters, C. L., F. W. Menk, and B. J. Fraser (1991), The resonance structure of low latitude pc3 geomagnetic pulsations, *Geophys. Res. Lett.*, *18*(12), 2293.

Waters, C. L., F. W. Menk, and B. J. Fraser (1994), Low latitude geomagnetic field line resonance: experiment and modeling, *J. Geophys. Res.*, *99*(A9), 17,547.

Yeh, H.-C., and J. C. Foster (1990), Storm time heavy ion outflow at mid-latitude, *J. Geophys. Res.*, *95*(A6), 7881.

D. Berube and M. B. Moldwin, Department of Earth and Space Sciences, Institute of Geophysics and Planetary Physics, University of California, Los Angeles, 595 Charles Young Drive E, Los Angeles, CA 90095-1567, USA. (dberube@igpp.ucla.edu)

S. F. Fung, NASA Goddard Space Flight Center, Code 632, Greenbelt, MD 20771, USA.

J. L. Green, NASA Goddard Space Flight Center, Code 630, Greenbelt, MD 20771, USA.